The Characteristics of the $(\alpha V^{371}C)_3(\beta R^{337}C)_3\gamma$ Double Mutant Subcomplex of the TF_1-ATPase Indicate that the Catalytic Site at the $\alpha_{TP}-\beta_{TP}$ Interface with Bound MgADP in Crystal Structures of MF_1 Represents a Catalytic Site Containing Inhibitory MgADP†

Sanjay Bandyopadhyay,‡ Eiro Muneyuki,§ and William S. Allison*,‡

Department of Chemistry and Biochemistry, University of California at San Diego, La Jolla, California 92093-0601, and Chemical Resources Laboratory, Tokyo Institute of Technology, Nagatsuta 4259, Yokohama 226-8503, Japan

Received October 28, 2004; Revised Manuscript Received December 7, 2004

ABSTRACT: In the MF_1 crystal structure with the MgADP−fluoroaluminate complex bound to two catalytic sites [Menz, R. I., Walker, J. E., and Leslie, A. G. W. (2001) *Cell 106,* 331−341], the guanidinium of βR^{337} is within 2.9 Å of the α-oxygen of αS^{370} and 3.7 Å of a methyl group of αV^{371} at the $\alpha_E-\beta_{HC}$ interface. To examine the functional role of this contact, the $(\alpha V^{371}C)_3(\beta R^{337}C)_3\gamma$ subcomplex of the TF_1-ATPase was prepared and characterized. Steady state ATPase activity of the reduced double-mutant is 30% of that of the wild type. Inactivation of the double mutant containing empty catalytic sites or MgADP bound to one catalytic site with $CuCl_2$ cross-linked two $\alpha-\beta$ pairs, whereas a single $\alpha-\beta$ pair cross-linked when at least two catalytic sites contained MgADP. The reduced double mutant hydrolyzed substoichiometric ATP 100-fold more rapidly than the enzyme containing two cross-linked $\alpha-\beta$ pairs. Addition of $AlCl_3$ and NaF to the reduced double mutant after incubation with stoichiometric MgADP or 200 μM MgADP irreversibly inactivated the steady state ATPase activity with rate constants of 1.5×10^{-2} and 4.1×10^{-2} min^{-1}, respectively. In contrast, addition of $AlCl_3$ and NaF to the cross-linked enzyme after incubation with stoichiometric or 200 μM MgADP irreversibly inactivated ATPase activity with a common rate constant of $\sim 10^{-4}$ min^{-1}. Correlation of these results with crystal structures of MF_1 suggests that the catalytic site at the $\alpha_{TP}-\beta_{TP}$ interface is loaded first upon addition of nucleotides to nucleotide-depleted F_1-ATPases and that the catalytic site at the $\alpha_{TP}-\beta_{TP}$ interface with bound MgADP in crystal structures represents a catalytic site containing inhibitory MgADP.

The proton-translocating F_0F_1-ATP synthases are membrane protein complexes comprised of two molecular motors that are connected by a common rotor. The F_0 component is an integral membrane protein complex that translocates protons, whereas F_1 is a peripheral membrane protein complex containing three catalytic sites. During ATP synthesis, proton translocation through F_0 impels rotation of the rotor, which drives condensation of ADP with P_i at the catalytic sites of F_1 that operate sequentially in a highly cooperative manner (*1*).

When removed from the membrane as a soluble complex, F_1 contains five different subunits in an $\alpha_3\beta_3\gamma\delta\epsilon$ stoichiometry and has substantial ATPase activity. In crystal structures of F_1, the α and β subunits are arranged alternately in a hexameric array that surrounds an antiparallel coiled coil comprised of the amino- and carboxyl-terminal α helices of the γ subunit (*2*−*4*). In the original crystal structure of MF_1[1] (*2*), catalytic sites are heterogeneously liganded and are located mostly on β subunits at $\alpha-\beta$ interfaces. One catalytic site, called β_{TP}, contains MgAMP-PNP; a second catalytic site, called β_{DP}, contains MgADP, and a third catalytic site, called β_E, is empty. Whereas β_{TP} and β_{DP} have closed conformations, β_E has an open conformation. The α subunits contributing to catalytic sites on β_{TP}, β_{DP}, and β_E are designated α_{TP}, α_{DP}, and α_E, respectively. F_1 has three additional nucleotide binding sites, called noncatalytic sites. In the original crystal structure of bovine MF_1 (*2*), noncatalytic sites are homogeneously liganded with MgAMP-PNP and are located mostly on α subunits at $\alpha-\beta$ interfaces that differ from the interfaces that comprise catalytic sites.

Several point mutants of the *Escherichia coli* ATP synthase have been described that are located at $\alpha-\beta$ interfaces near catalytic sites which have defective synthetic and hydrolytic activities (*5*−*8*). Noumi et al. (*5*) demonstrated that isolated EF_1 containing the $\alpha S^{370}F$ substitution[2] hydrolyzes substoichiometric ATP (unisite ATPase activity) at a rate comparable to that of the wild type, but has severely attenuated multisite ATPase activity. Subsequently, Lee et al. (*8*) demonstrated that the multisite ATPase activity of

† This work was supported by National Institute of General Medical Sciences Grant GM 16974 from the National Institutes of Health.

* To whom correspondence should be addressed. Telephone: (858) 534-3057. Fax: (858) 822-0079. E-mail: wsa@checfs2.ucsd.edu.

‡ University of California at San Diego.

§ Tokyo Institute of Technology.

[1] Abbreviations: MF_1, TF_1, and EF_1, F_1-ATPases from bovine heart mitochondria, the thermophilic *Bacillus* PS3, and *E. coli*, respectively; AMP-PNP, 5′-adenylyl-β,γ-imidophosphate; LDAO, lauryldimethylamine oxide; DTT, dithiothreitol; DCCD, *N*,*N*′-dicyclohexylcarbodiimide.

10.1021/bi047694z CCC: $30.25
Published on Web 01/28/2005

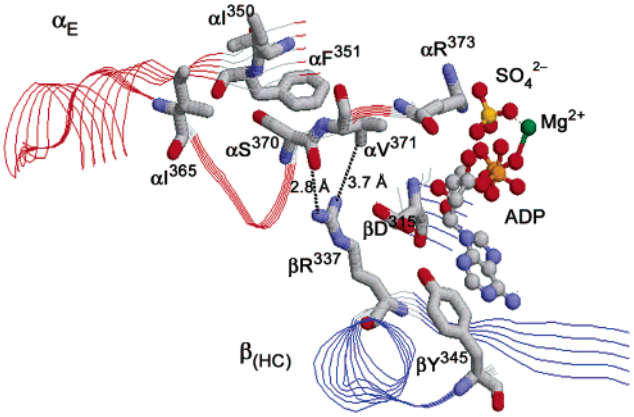

FIGURE 1: Relative positions of the side chains of αS^{370}, αV^{371}, and βR^{337} in the crystal structure of the $(MgADP{\cdot}AlF_4^-)_2{-}MF_1$ complex. This figure was constructed from the coordinates of MF_1 obtained from Protein Data Bank entry 1H8E (*4*) using RasMol provided by R. Sayle (Glaxo Wellcome Research and Development, Greenford, U.K.).

the $\alpha S^{370}C$ mutant of EF_1 is 30% of that of the wild type. They also showed that modification of only one of the introduced cysteines with *N*-ethylmaleimide was sufficient to abolish multisite ATPase activity without affecting unisite ATPase activity. From these characteristics, Lee et al. (*8*) concluded that introduction of a bulky side chain in the position occupied by $\alpha S^{370}C$ interferes with $\alpha{-}\beta$ interactions that participate in positive catalytic site cooperativity. However, the molecular basis for this behavior was not apparent until Menz et al. (*4*) reported the crystal structure of MF_1 containing MgADP−fluoroaluminate complexes bound to two catalytic sites.

In the crystal structure reported by Menz et al. (*4*), two closed catalytic sites contain bound MgADP−fluoroaluminate complexes and the third catalytic site is "half-closed" and contains bound MgADP and sulfate. The half-closed catalytic site is designated β_{HC}. Figure 1 illustrates that the guanidinium of βR^{337} is within 2.9 Å of the α-oxygen of αSer^{370} (not the oxygen in the side chain) and within 3.7 Å of one of the methyl groups of αV^{371} at the $\alpha_E{-}\beta_{HC}$ interface near the adenine of ADP bound to β_{HC}. The guanidinium of βR^{337} is more distant from the α-oxygen of αS^{370} and the side chain of αV^{371} at all other $\alpha{-}\beta$ interfaces in all crystal structures of MF_1 as shown in Table 1 for representative crystal structures. To test the possibility that the unique arrangement of the guanidinium of βR^{337} with respect to αS^{370} and αV^{371} at the $\alpha_E{-}\beta_{HC}$ interface represents a transient contact that occurs during cooperative, multisite ATP hydrolysis, the $(\alpha V^{371}C)_3(\beta R^{337}C)_3\gamma$ double mutant has been prepared and its catalytic properties have been characterized before and after cross-linking the introduced cysteines with $CuCl_2$. Since the side chain of αS^{370} is distant and points away from the guanidinium of βR^{337} at the $\alpha_E{-}\beta_{HC}$ interface as shown in Figure 1, αV^{371} rather than αS^{370} was substituted with cysteine.

[2] Unless stated otherwise, residue numbers of MF_1 are used throughout. In TF_1, αS^{362} and αV^{363} are equivalent to αS^{370} and αV^{371}, respectively, in MF_1. In TF_1, αI^{342}, αF^{343}, αI^{357}, and αC^{193} are equivalent to αI^{350}, αF^{351}, αI^{365}, and αC^{201}, respectively, of MF_1. In TF_1, βD^{311}, βR^{333}, and βY^{341} are equivalent to βD^{315}, βR^{337}, and βY^{345}, respectively, in MF_1. In EF_1, αS^{373} and βY^{331} are equivalent to αS^{370} and βY^{345}, respectively, in MF_1.

Table 1: Distances (angstroms) between the Guanidinium of βR^{337} and the α-Oxygen of αS^{370} and a Methyl Group of αV^{371} in Crystal Structures of MF_1

crystal structure	interface	αS^{370} $O_\alpha{-}$ βR^{337} N_H	αV^{371} $C_\gamma{-}$ βR^{337} N_H
frozen native[a]	$\alpha_E{-}\beta_E$	7.05	5.04
frozen native[a]	$\alpha_T{-}\beta_T$	11.45	10.51
frozen native[a]	$\alpha_D{-}\beta_D$	8.35	6.68
$(MgADP{\cdot}AlF_4^-)_2$[b]	$\alpha_E{-}\beta_{HC}$	2.85	3.69
$(MgADP{\cdot}AlF_4^-)_2$[b]	$\alpha_T{-}\beta_T$	11.04	10.76
$(MgADP{\cdot}AlF_4^-)_2$[b]	$\alpha_D{-}\beta_D$	8.53	6.98
DCCD[c]	$\alpha_E{-}\beta_E$	7.36	4.89
DCCD[c]	$\alpha_T{-}\beta_T$	11.77	9.58
DCCD[c]	$\alpha_D{-}\beta_D$	8.35	7.21

[a] Obtained from Protein Data Bank entry 1E1Q. [b] Obtained from Protein Data Bank entry 1H8E. [c] Obtained from Protein Data Bank entry 1E79.

EXPERIMENTAL PROCEDURES

Generation and Expression of Mutant Plasmids. The expression plasmid pKK, which carries the genes encoding α, β, and γ subunits of the TF_1-ATPase, was used for both site-directed mutagenesis and gene expression (*9*). Site-specific substitutions in the wild-type pKK expression plasmid were performed with PCR using the QuikChange site-directed mutagenesis kit from Stratagene. The $\alpha V^{371}C$ single mutant was generated with the mutagenic oligonucleotides 5′-CAGGGTTGTCCTGTTCGCGCGTCGG-3′ and its corresponding complement (not shown) using the wild-type pKK plasmid as a template. The changed bases are underlined. The $\beta R^{337}C$ single mutant plasmid DNA (*10*) was used as a template to generate the $\alpha V^{371}C/\beta R^{337}C$ double mutant. After transformation in *E. coli* strain JM109, plasmids were purified using the Wizard *Plus* miniprep kit from Promega and the mutations were confirmed by DNA sequence analysis. The mutant plasmids were expressed in *E. coli* strain JM103 (*unc*−). The wild-type $\alpha_3\beta_3\gamma$ and mutant subcomplexes were purified and stored as suspensions in 75% saturated ammonium sulfate at 4 °C as described by Matsui and Yoshida (*9*).

Preparation of the Reduced and Cross-Linked Forms of the $(\alpha V^{371}C)_3(\beta R^{337}C)_3\gamma$ *Double Mutant Subcomplex.* The $(\alpha V^{371}C)_3(\beta R^{337}C)_3\gamma$ double mutant was isolated in partially cross-linked form as assessed by SDS−PAGE. After CDTA treatment, the isolated $(\alpha V^{371}C)_3(\beta R^{337}C)_3\gamma$ double mutant subcomplex, at 1 mg/mL in 50 mM Tris-HCl (pH 8.0) containing 0.1 mM EDTA, was completely reduced with 10 mM DTT. Immediately before cross-linking, DTT was removed by passing samples through centrifuge columns of Sephadex G-50 equilibrated with 50 mM Tris-HCl (pH 8.0) (*11*). Cross-linking was then performed by treating the reduced double mutant enzyme, at 1 mg/mL, with 1 or 100 μM $CuCl_2$ for the times indicated in specific experiments. $CuCl_2$ was then removed by passing 100 μL samples of the reaction mixtures through 1 mL centrifuge columns of Sephadex G-50 that were equilibrated and eluted with 50 mM Tris-HCl (pH 8.0).

Analytical Methods. Before kinetic measurements and cross-linking, endogenous nucleotides were removed from the isolated wild type and reduced $\alpha V^{371}C/\beta R^{337}C$ double mutant subcomplexes by treating them at 1 mg/mL in 50 mM Tris-HCl buffer (pH 8.0) with 10 mM CDTA as described in detail previously (*12*). The CDTA-treated

enzyme subcomplexes were essentially free of endogenously bound nucleotides as assessed by HPLC.

Multisite ATPase activity was determined spectrophotometrically in assay medium containing 2 mM ATP and 3 mM Mg^{2+} in 50 mM HEPES-KOH (pH 8.0) at 30 °C using an ATP regeneration system coupled to oxidation of NADH described previously (*13*). Protein concentrations were determined by the method of Bradford using Coomassie *Plus* reagent from Pierce (*14*).

Hydrolysis of substoichiometric ATP by the $\alpha V^{371}C/\beta R^{337}C$ double mutant was examined by vigorously vortexing 50 μL of 1.3 μM reduced or cross-linked enzyme with 50 μL of 0.5 μM ATP and 1 mM $MgCl_2$ in 50 mM Tris-HCl (pH 8.0) at room temperature. At 0, 10, 20, 40, 60, and 90 s, 5 μL of 24% perchloric acid was added to the reaction mixtures. After the mixture had been chilled on ice, 5 μL of 5 M K_2CO_3 was added. Denatured protein and precipitated $KClO_4$ were then removed by centrifugation, and the amounts of ADP and ATP in the supernatants were determined by reversed-phase HPLC on a TOSOH TSK gel (ODS-80Ts) column that was eluted isocratically with 0.1 M sodium phosphate (pH 6.9) containing 1 mM EDTA.

Analysis of the $\alpha-\beta$ Cross-Links by SDS−PAGE. SDS−PAGE was performed on 12% Tris-HCl Ready Gels from Bio-Rad at 200 V for 40 min. Samples containing 6 μg of the reduced or oxidized double mutant in buffer containing 62.5 mM Tris-HCl (pH 6.8), 10% glycerol, 0.025% bromophenol blue, and 2% SDS were applied to the gels. After the gels had been stained with 0.1% Coomassie Blue and then thoroughly destained, gels were photographed with a photodocumentation Polaroid camera. The photographs were scanned with an EPSON Perfection 1250 scanner, and the free and cross-linked α and β subunits were quantified using GelExpert software from Nucleotech.

Comparison of the Affinities of the Reduced and Cross-Linked Forms of the $(\alpha V^{371}C)_3(\beta R^{337}C)_3\gamma$ Double Mutant for MgADP. The affinity of the high-affinity catalytic site in the reduced and cross-linked forms of the $\alpha V^{371}C/\beta R^{337}C$ double mutant was estimated in the following manner. To obtain the desired concentrations of ADP, 5 μL of ADP solutions at different concentrations was added to 95 μL of 1.0 μM reduced or cross-linked enzyme in 50 mM Tris-HCl containing 1 mM $MgCl_2$. After incubation for 10 min at room temperature, the mixtures were applied to 1 mL centrifuge columns of Sephadex G-50 fine (*14*) that were equilibrated and eluted with 50 mM Tris-HCl (pH 8.0) containing 1 mM $MgCl_2$. After the eluates had been diluted to 120 μL with the same buffer, the UV spectrum was scanned to determine the protein concentration. Then 6 μL of 24% perchloric acid was added to the samples which were placed on ice for several minutes before addition of 6 μL of 5 M K_2CO_3. After removal of the denatured protein and precipitated $KClO_4$ by centrifugation, the amount of bound ADP was determined by submitting 70 μL samples of the supernatants to reversed-phase HPLC on a TOSOH TSK gel ODS-80Ts column that was equilibrated and eluted with 0.1 M sodium phosphate (pH 6.9) containing 1 mM EDTA.

RESULTS

Cross-Linking the Introduced Cysteines in the $(\alpha V^{371}C)_3(\beta R^{337}C)_3\gamma$ Double Mutant Inactivates Steady State ATP Hydrolysis and Severely Impairs Hydrolysis of Substoichiometric ATP. The steady state ATPase activities of the wild type and $\alpha V^{371}C$ and $\beta R^{337}C$ single mutants and the reduced $\alpha V^{371}C/\beta R^{337}C$ double mutant subcomplexes are compared in Table 2. Both the $\alpha V^{371}C$ and $\beta R^{337}C$ single mutants hydrolyze 2 mM ATP at ~50% of the wild-type rate, whereas the fully reduced $\alpha V^{371}C/\beta R^{337}C$ double mutant, freshly prepared as described in Experimental Procedures, hydrolyzes 2 mM ATP at ~30% of the wild-type rate. Since the wild-type $\alpha_3\beta_3\gamma$ subcomplex is stimulated 4-fold by including 0.06% LDAO in the assay medium (*15*, *16*), the extent of stimulation of the mutant subcomplexes by 0.06% LDAO is also included in the comparison. LDAO reduces the propensity of the wild-type enzyme to entrap inhibitory MgADP in a catalytic site during turnover. Table 2 shows that LDAO stimulates the ATPase activity of the single and reduced double mutant subcomplexes to a significantly lesser extent than it stimulates the wild-type subcomplex. This suggests that the attenuated ATPase activity of the mutant enzymes, compared to that of the wild type, is not caused by an increased propensity to entrap inhibitory MgADP in a catalytic site during turnover.

Table 2: Comparison of the ATPase Activities of the Wild Type, $\alpha V^{371}C$ and $\beta R^{337}C$ Single Mutant Subcomplexes, and the Reduced and Cross-Linked $\alpha V^{370}C/\beta R^{337}C$ Double Mutant Subcomplex

subcomplex	specific activity (μmol min^{-1} mg^{-1})	activation by LDAO
$\alpha_3\beta_3\gamma$	20	4.1-fold
$\alpha(V^{371}C)_3\beta_3\gamma$	10.5	2.1-fold
$\alpha_3(\beta R^{337}C)_3\gamma$	9.7	1.1-fold
reduced $(\alpha V^{371}C)_3(\beta R^{337}C)_3\gamma$[a]	6.5	2.4-fold
cross-linked $(\alpha V^{371}C)_3(\beta R^{337}C)_3\gamma$[b]	0.15	2.5-fold

[a] The steady state ATPase activity was determined immediately after removal of DTT from the fully reduced enzyme as described in Experimental Procedures. [b] The cross-linked double mutant was prepared after treatment of the fully reduced enzyme with 1 μM $CuCl_2$ for 1 h, at which time Cu^{2+} ion was removed as described in Experimental Procedures.

Table 2 also shows that treatment of the reduced $\alpha V^{371}C/\beta R^{337}C$ double mutant with 1 μM $CuCl_2$ for 1 h inactivates ATPase activity by 98%. In addition to the introduced cysteines, the double mutant subcomplex contains three Cys residues at position 193 in α subunits which corresponds to αC^{201} of MF_1. In crystal structures of MF_1, the sulfur in the side chain of αC^{201} in each α subunit is at least 21 Å from the side chain of αV^{371} in any of the α subunits or the side chain of βR^{337} in any of the β subunits. Therefore, the inactivation observed upon treatment of the reduced double mutant with $CuCl_2$ reflects cross-linking of the introduced cysteines. LDAO stimulates the ATPase activity of the $CuCl_2$-treated enzyme and the fully reduced enzyme by the same percentage. This suggests that the 2% residual ATPase activity observed after treatment with $CuCl_2$ reflects incomplete cross-linking of the introduced cysteines.

When 0.5 μmol of ATP was rapidly mixed with an equal volume containing 1.3 μmol of the fully reduced double mutant in the presence of 1 mM Mg^{2+}, all of the ATP was hydrolyzed within 10 s. In contrast, under the same conditions, the cross-linked double mutant hydrolyzed substoichiometric ATP with a half-time of 15.5 s. As determined from the semilogarithmic plot in Figure 2, this corresponds to a k_{cat} of 4.5×10^{-2} s^{-1}. Table 3 shows that 0.6 mol of

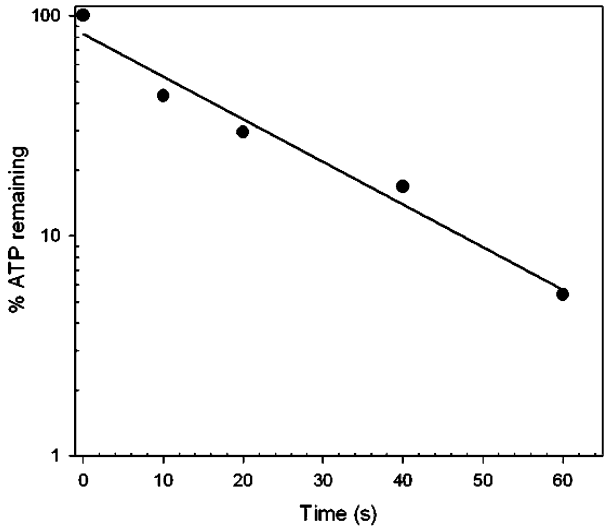

FIGURE 2: Rate of hydrolysis of substoichiometric ATP by the cross-linked $(\alpha V^{371}C)_3(\beta R^{337}C)_3\gamma$ subcomplex. The reaction mixture was prepared and analyzed for ATP hydrolysis as described in Experimental Procedures. In these experiments, 100 μM $CuCl_2$ was used to convert the fully reduced double mutant to the cross-linked form. The Cu^{2+} ion was removed before ATP hydrolysis was examined as described in Experimental Procedures. The semilogarithmic plot indicates a $t_{0.5}$ of 15.5 s which corresponds to a k_{cat} of 4.5×10^{-2} s^{-1}.

Table 3: Comparison of Binding of MgADP to the Reduced and Cross-Linked Forms of the $(\alpha V^{371}C/\beta R^{337}C)$ Double Mutant[a]

MgADP added (μM)	cross-linked double mutant[b] (mol of ADP/mol of enzyme)	reduced double mutant[c] (mol of ADP/mol of enzyme)
0.3	0.22	0.28
0.5	0.38	0.54
1.0	0.59	0.85
1.0	0.66	0.86
1.5	0.68	1.14
2.0	0.80	1.35
3.0	0.95	1.84

[a] The amount of bound MgADP was determined as described in detail in Experimental Procedures. [b] The cross-linked double mutant was prepared by treating the reduced double mutant with 100 μM $CuCl_2$ for 2 h at room temperature, at which time the Cu^{2+} ion was removed as described in Experimental Procedures. [c] The fully reduced double mutant was prepared immediately before use in these experiments as described in Experimental Procedures.

ADP remained bound per mole of the cross-linked double mutant after addition of stoichiometric MgADP to it followed by passage through a centrifuge column of Sephadex G-50 (*11*). Under the same conditions, 0.85 mol of ADP remained bound per mole of the reduced double mutant. Although the binding data indicate that the cross-linked double mutant retained somewhat less ADP than the fully reduced form, the difference is small and does not appear to account for the slow rate of hydrolysis of substoichiometric ATP. Figure 2 clearly shows that hydrolysis of substoichiometric ATP by the cross-linked enzyme is a first-order process. Therefore, the slow rate of hydrolysis of substoichiometric ATP by the cross-linked enzyme reflects a defective hydrolytic step rather than defective binding of MgATP to the highest-affinity catalytic site.

The Number of $\alpha-\beta$ *Pairs Cross-Linked upon Treatment of the Reduced* $\alpha V^{371}C/\beta R^{337}C$ *Mutant with* $CuCl_2$ *Depends on the Number of Catalytic Sites that Contain MgADP.* Figure 3 illustrates the rates of inactivation of the reduced

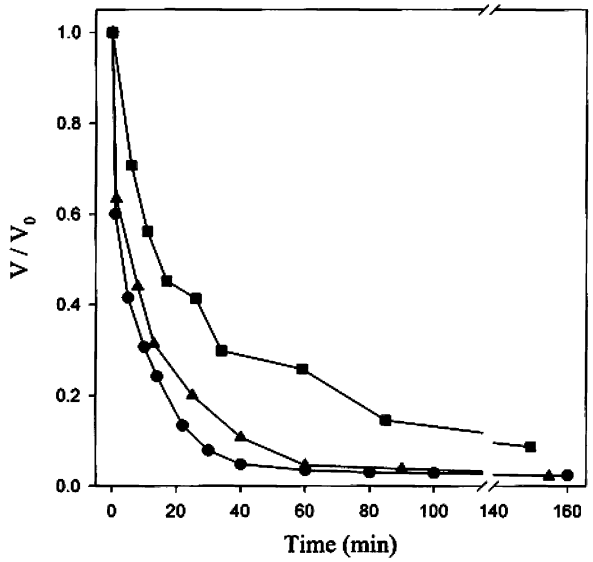

FIGURE 3: Rates of inactivation of the reduced $(\alpha V^{371}C)_3(\beta R^{337}C)_3\gamma$ double mutant subcomplex by $CuCl_2$ in the presence and absence of MgADP. After complete reduction of the double mutant subcomplex as described in Experimental Procedures, excess DTT and EDTA were removed by passing 100 μL samples of the protein solutions through 1 mL centrifuge columns of Sephadex G-50 equilibrated with 50 mM Tris-HCl (pH 8.0). The inactivation mixtures contained the reduced double mutant, at 1 mg/mL (2.85 μM), in 50 mM Tris-HCl (pH 8.0): (●) with 1 μM $CuCl_2$, (▲) with 2.85 μM ADP and 1 mM Mg^{2+} followed by 1 μM $CuCl_2$, and (■) with 200 μM ADP and 1 mM Mg^{2+} followed by 1 μM $CuCl_2$. At the indicated times, 10 μL samples of the inactivation mixtures were removed and assayed for ATPase activity.

$(\alpha V^{371}C)_3(\beta R^{337}C)_3\gamma$ double mutant by $CuCl_2$ in the presence and absence of different concentrations of MgADP. When the reduced double mutant was treated with 1 μM $CuCl_2$ in the absence of MgADP, nearly complete inactivation of ATPase activity occurred within 1 h (●). Essentially the same rate and extent of inactivation were observed when the reduced enzyme was treated with 1 μM $CuCl_2$ under the same conditions in the presence of stoichiometric MgADP (▲). In contrast, in the presence of 200 μM MgADP, the rate of inactivation promoted by 1 μM $CuCl_2$ was slower (■) than the rate observed in the presence of stoichiometric MgADP (▲). In another experiment (not illustrated), it was shown that treatment of the fully reduced double mutant with 1 μM $CuCl_2$ in the absence of MgADP led to 98% inactivation within 1 h, whereas 2.5 h was required to attain 95% inactivation when the fully reduced enzyme was treated with 1 μM $CuCl_2$ in the presence of 200 μM MgADP.

Figure 4 shows the extent of cross-linking of α and β subunits that was observed when samples of the reaction mixtures described in the legend of Figure 3 were submitted to SDS−PAGE after maximal inactivation had been attained. The distributions of cross-linked and free α and β subunits were essentially the same in lane 2, which represents the inactivation mixture without MgADP, and lane 3, which represents the inactivation mixture containing stoichiometric MgADP. In contrast, lane 4 shows that the distribution of cross-linked and free α and β subunits differed significantly when inactivation with $CuCl_2$ was performed in the presence of 200 μM MgADP. Analysis of band intensities in the gel as described in Experimental Procedures revealed that oxidation of the reduced double mutant with $CuCl_2$ in the presence (lane 3) and absence (lane 2) of stoichiometric

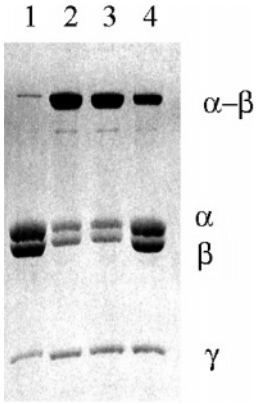

FIGURE 4: Resolution of $\alpha-\beta$ cross-links by SDS−PAGE. When maximal inactivation was attained, $CuCl_2$ was removed from the inactivation mixtures described in the legend of Figure 3 by passing 70 μL samples through 1 mL centrifuge columns of Sephadex G-50 equilibrated with 50 mM Tris-HCl buffer (pH 8.0) containing 0.1 mM EDTA. The samples containing inactivated enzyme free of Cu^{2+} were treated immediately with 4 mM *N*-ethylmaleimide for 15 min at 23 °C. Then, fractions of each sample containing 6 μg of protein were mixed with buffer containing SDS and applied to a 12% polyacrylamide gel which was submitted to electrophoresis as described in Experimental Procedures: lane 1, reduced enzyme with 10 mM DTT; lane 2, reduced enzyme with 1 μM $CuCl_2$; lane 3, reduced enzyme with 1 mM $MgCl_2$ and 2.85 μM ADP followed by 1 μM $CuCl_2$; and lane 4, reduced enzyme with 1 mM $MgCl_2$ and 200 μM ADP followed by 1 μM $CuCl_2$.

MgADP led to 64 and 66% cross-linking, respectively, whereas oxidation in the presence of 200 μM MgADP led to 31% cross-linking (lane 4). Therefore, two $\alpha-\beta$ pairs were cross-linked in the absence of MgADP or in the presence of stoichiometric MgADP, whereas only a single $\alpha-\beta$ pair was cross-linked more slowly in the presence of 200 μM MgADP.

Cross-Linking Two $\alpha-\beta$ Pairs in the $\alpha V^{371}C/\beta R^{337}C$ Double Mutant Significantly Reduces the Rate of Formation of MgADP−Fluoroaluminate Complexes in Catalytic Sites. Figure 5A illustrates the rates of inactivation observed upon addition of $AlCl_3$ and NaF to solutions of the reduced $\alpha V^{371}C/\beta R^{337}C$ double mutant containing either stoichiometric MgADP (▲) or 200 μM MgADP (●). The first-order rate constants for these inactivations are 4.1×10^{-2} and 1.5×10^{-2} min^{-1}, respectively. The rate of inactivation represents the rate of assembly of MgADP−fluoroaluminate complexes. Therefore, MgADP−fluoroaluminate complexes assemble ~3-fold faster when multiple catalytic sites of the reduced double mutant enzyme contain MgADP as opposed to when a single catalytic site contains bound MgADP.

In contrast, Figure 5B shows that after incubation of the cross-linked $\alpha V^{371}/\beta R^{337}C$ mutant with either stoichiometric MgADP or 200 μM MgADP for 30 min followed by addition of $AlCl_3$ and NaF, ATPase activity was irreversibly inactivated with a rate constant of less than 2×10^{-4} min^{-1}. Table 3 shows that incubation of the cross-linked $\alpha V^{371}/\beta R^{337}C$ mutant with 200 μM MgADP is sufficient to saturate a single catalytic site with MgADP.

The experimental points in Figure 5B were determined by assaying the ATPase activity of the cross-linked enzyme at the times indicated in the presence of 10 mM DTT. Under these conditions, the disulfide bond in the cross-linked enzyme was reduced virtually instantaneously. Please note that the time coordinate of Figure 5B is hours, whereas the time coordinate of Figure 5A is minutes.

DISCUSSION

Since the $\beta R^{337}C$ single mutant and the $\alpha V^{371}C/\beta R^{337}C$ double mutant subcomplexes hydrolyze 2 mM ATP at 50 and 30%, respectively, of the rate exhibited by the wild-type subcomplex, it is clear that transient formation of the apparent hydrogen bond between the carbonyl oxygen of αS^{370} and the guanidinium of βR^{337} at the $\alpha_E-\beta_{HC}$ interface in the $(MgADP{\cdot}AlF_4^-)_2-MF_1$ crystal structure (*4*) illustrated in Figure 1 is not essential for ATP hydrolysis. However, cross-linking the introduced cysteines in one or two $\alpha-\beta$ pairs abolishes steady state ATP hydrolysis. This indicates that during steady state ATP hydrolysis, the side chains of αV^{371} and βR^{337} cycle through the three different conformations observed in crystal structures that are summarized in Table 1.

Figure 1 also shows that the side chain of αS^{370} is surrounded by hydrophobic side chains contributed by other amino acid residues in the α subunit that are highly conserved. In the $\alpha_E-\beta_{HC}$ catalytic site depicted in Figure 1, the guanidinium in the side chain of αR^{373} is hydrogen bonded to the β-phosphate of the bound ADP. In the $\alpha_{TP}-\beta_{TP}$ and $\alpha_{DP}-\beta_{DP}$ catalytic sites in the $(MgADP{\cdot}AlF_4^-)_2-MF_1$ crystal structure, the guanidinium of αR^{373} is hydrogen bonded to fluorine atoms of the AlF_4^- moiety, indicating that it has a direct role in catalysis (*4*). Therefore, it is possible that failure of the $\alpha S^{370}F$ mutant of EF_1 to catalyze multisite ATP hydrolysis (*6*, *7*) is caused by hydrophobic interactions of the introduced phenylalanine with the neighboring side chains. The putative interactions could immobilize this region of the α subunit in a manner that prevents participation of αR^{373} in cooperative ATP hydrolysis. The observation that derivatization of a single introduced Cys in the $\alpha S^{370}C$ mutant of EF_1 is sufficient to prevent multisite ATP hydrolysis is consistent with this argument (*8*).

Table 1 shows that the side chain of αV^{371} is more distant from the side chain of βR^{337} at the $\alpha_{TP}-\beta_{TP}$ interface than at the $\alpha_E-\beta_{HC}$ and $\alpha_{DP}-\beta_{DP}$ interfaces in the $(MgADP{\cdot}AlF_4^-)_2-MF_1$ crystal structure (*4*) as well as at the $\alpha_E-\beta_E$ and $\alpha_{DP}-\beta_{DP}$ interfaces in other crystal structures of MF_1. Figure 4 clearly shows that two $\alpha-\beta$ pairs cross-linked upon treatment of the reduced $(\alpha V^{371}C)_3(\beta R^{337}C)_3\gamma$ double mutant with $CuCl_2$ after a single catalytic site had been loaded with stoichiometric MgADP, whereas only a single $\alpha-\beta$ pair cross-linked after at least two catalytic sites had been loaded with MgADP. These observations indicate that the catalytic site at the $\alpha_{TP}-\beta_{TP}$ interface in crystal structures loads first upon addition of nucleotides and Mg^{2+} ion to F_1-ATPases free of nucleotides. Correlation of the nucleotide content of the $\alpha_{TP}-\beta_{TP}$ catalytic site in crystal structures of MF_1 with the conditions used to load catalytic sites with nucleotides prior to crystallization supports this tenet. Crystal structures of MF_1 containing MgAMP-PNP bound to the $\alpha_{TP}-\beta_{TP}$ catalytic site were determined after nucleotide-depleted enzyme had been loaded under the conditions described by Lutter et al. (*16*). According to this procedure, AMP-PNP and ADP were first added to nucleotide-depleted MF_1 in a 50:1 molar ratio in the presence of 8 mM $MgCl_2$ at pH 7.2. Under these conditions, it is reasonable to assume that the highest-affinity catalytic site for nucleotides binds MgAMP-PNP. In contrast, the crystals used to determine the DCCD−

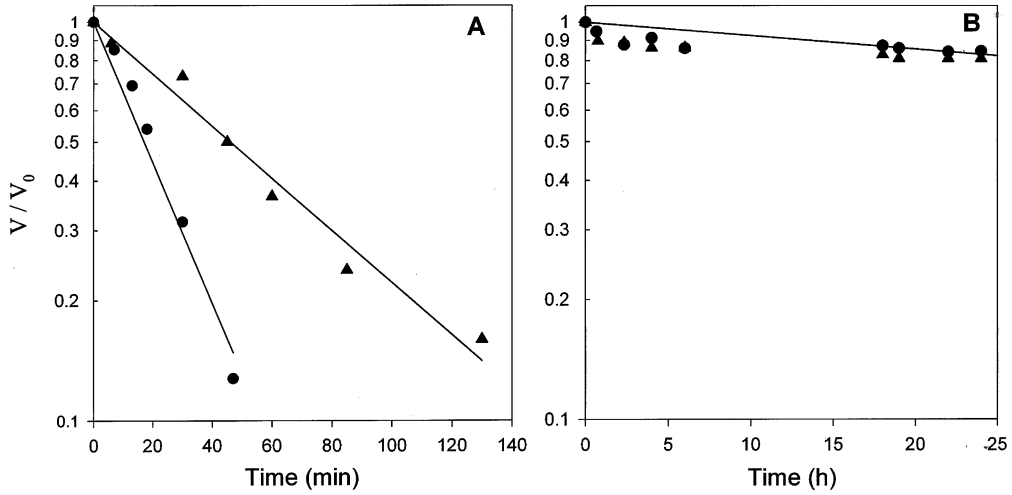

FIGURE 5: Rates of formation of MgADP−fluoroaluminate complexes in catalytic sites of the $(\alpha V^{371}C)_3(\beta R^{337}C)_3\gamma$ double mutant subcomplex before and after cross-linking. (A) The reduced $(\alpha V^{371}C)_3(\beta R^{337}C)_3\gamma$ double mutant subcomplex, at 1 mg/mL (2.85 μM), in 50 mM Tris-HCl buffer (pH 8.0) containing 10 mM DTT, 0.1 mM EDTA, and 2 mM $MgCl_2$ was incubated with 2.85 μM ADP (▲) or 200 μM ADP (●) for 30 min at 23 °C, at which time NaF and $AlCl_3$ were added to final concentrations of 5 mM and 200 μM, respectively. At the specified times, 10 μL samples were withdrawn and assayed for ATPase activity in the presence of 10 mM DTT as described in Experimental Procedures. (B) After removal of excess DTT and EDTA from the reduced enzyme solutions by passing 100 μL samples through 1 mL centrifuge columns of Sephadex G-50 equilibrated with 50 mM Tris-HCl (pH 8.0), the reduced double mutant was cross-linked with 1 μM $CuCl_2$ for 1 h as described in Experimental Procedures. After removal of $CuCl_2$ by passing the oxidized double mutant through 1 mL centrifuge columns of Sephadex G-50 equilibrated with 50 mM Tris-HCl (pH 8.0), the cross-linked enzyme was incubated with 2.85 (▲) or 200 μM (●) ADP with 2 mM $MgCl_2$ for 30 min at 23 °C, before addition of NaF and $AlCl_3$ to final concentrations of 5 mM and 200 μM, respectively. At the specified times, 10 μL samples were withdrawn and assayed for ATPase activity in the presence of 10 mM DTT.

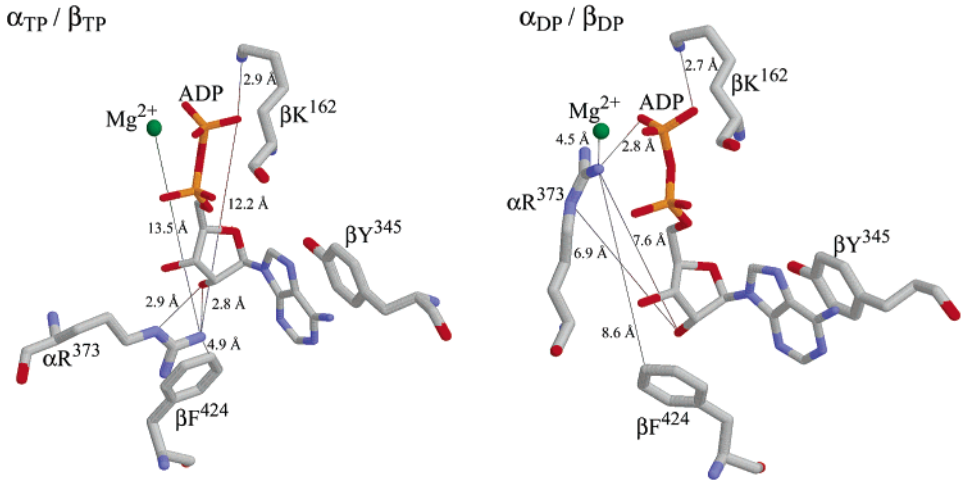

FIGURE 6: Different configurations of the side chain of αR^{373} in the $\alpha_{TP}-\beta_{TP}$ and $\alpha_{DP}-\beta_{DP}$ catalytic sites in the DCCD−MF_1 crystal structure. This figure was constructed from the coordinates of MF_1 obtained from Protein Data Bank entry 1E79 (*4*) using RasMol provided by R. Sayle (Glaxo Wellcome Research and Development).

MF_1 and $(ADP)_2-MF_1$ structures were prepared from nucleotide-depleted MF_1 that had been incubated with ADP only in the presence of Mg^{2+} ion (*3*, *17*). In the DCCD−MF_1 and $(ADP)_2-MF_1$ crystal structures, the guanidinium of αR^{373} is near the β-phosphate of ADP bound to the $\alpha_{DP}-\beta_{DP}$ catalytic site. However, in the $\alpha_{TP}-\beta_{TP}$ catalytic site of these crystal structures, the guanidinium of αR^{373} is hydrogen-bonded to the 2′-hydroxyl of the ribose of the bound ADP.

Figure 6 compares the different positions of the side chain of αR^{373} with respect to bound ADP, the Mg^{2+} ion, and βF^{424} at the $\alpha_{TP}-\beta_{TP}$ and $\alpha_{DP}-\beta_{DP}$ catalytic sites in the DCCD−MF_1 crystal structure (*3*). Whereas N_ϵ of αR^{373} is 2.95 Å from the 2′-hydroxyl of the ribose of ADP bound to the $\alpha_{TP}-\beta_{TP}$ catalytic site, the corresponding distance for the $\alpha_{DP}-\beta_{DP}$ catalytic site is 6.87 Å. Figure 6 also shows that the relative positions of N_H of αR^{373} with respect to the β-phosphate of ADP and the Mg^{2+} ion bound to the $\alpha_{TP}-\beta_{TP}$ and $\alpha_{DP}-\beta_{DP}$ catalytic sites have even greater discrepancies. The position of N_H in the αR^{373} side chain with respect to the phenyl group in the side chain of βF^{424} and the ϵ-amino group in the side chain of βK^{162} also differ significantly in the $\alpha_{TP}-\beta_{TP}$ and $\alpha_{DP}-\beta_{DP}$ catalytic sites in the DCCD−MF_1 crystal structure. Earlier, Kagawa et al. (Figure 3) showed that the positions of the side chain of αR^{373} with respect to the β-phosphate and the 2-hydroxyl of ADP and the side chains of βF^{424} and βK^{162} in the $\alpha_{TP}-\beta_{TP}$ and $\alpha_{DP}-\beta_{DP}$ catalytic sites of the $(ADP)_2-MF_1$ crystal structure have essentially the same deviations (*17*).

Given that the $\alpha_{TP}-\beta_{TP}$ catalytic site is loaded first upon addition of nucleotides and Mg^{2+} to F_1-ATPases free of nucleotides, it follows that the unusual arrangement of the side chain of αR^{373} with respect to ADP to the $\alpha_{TP}-\beta_{TP}$

catalytic site in the DCCD−MF_1 and $(ADP)_2$−MF_1 crystal structures (*3*, *17*) represents the configuration of a catalytic site containing inhibitory MgADP. Entrapment of inhibitory MgADP in a single catalytic site occurs directly upon binding of MgADP to nucleotide-depleted F_1-ATPases. Inhibitory MgADP is also entrapped in a catalytic site when nucleotide-depleted F_1-ATPases hydrolyze ATP in a single catalytic site (*15*, *18*−*21*). Masaike et al. (*22*) demonstrated that hydrolysis of ATP in a single catalytic site of the $\alpha_3(\beta R^{337}W)_3\gamma$ subcomplex of TF_1 occurred with a k_{cat} of 14.4 s^{-1}. Following hydrolysis, P_i dissociated with a rate constant of 2.8 s^{-1}. After the release of P_i, the mutant enzyme converted to the MgADP-inhibited form with a rate constant of 6.7×10^{-2} s^{-1}. This probably represents the rate of rearrangement of the guanidinium of αR^{373} from the dissociating P_i to the 2′-hydroxyl of the bound ADP.

Figure 5A shows that the MgADP−fluoroaluminate complex assembles in two catalytic sites of the reduced $\alpha V^{371}C/\beta R^{337}C$ double mutant more rapidly than it assembles in a single catalytic site. The same behavior was observed in a previous study with wild-type and mutant $\alpha_3\beta_3\gamma$ subcomplexes of TF_1 and nucleotide-depleted MF_1 (*23*). Therefore, formation of ADP−fluoroaluminate complexes in two catalytic sites is a cooperative process. The earlier study also showed that Mg[^{3}H]MgADP−fluoroaluminate complexes assembled more rapidly in two catalytic sites of the reduced forms of the $\alpha A^{396}C/\gamma A^{22}C$ and the $\beta D^{390}C/\gamma S^{90}C$ double mutants than a fluoroaluminate complex assembled in a single catalytic site. However, after $\alpha-\gamma$ or $\beta-\gamma$ cross-linking in these double mutants had occurred, the [^{3}H]MgADP−fluoroaluminate complex assembled in only a single catalytic site at the same rate observed when one or two catalytic sites contained [^{3}H]MgADP before addition of $AlCl_3$ and NaF. Therefore, rotation of the γ subunit is required for cooperative assembly of MgADP−fluoroaluminate complexes in two catalytic sites. In contrast, assembly of the MgADP−fluoroaluminate complex in a single catalytic site is not coupled to rotation of the γ subunit.

The following argument is proposed to explain the faster rate of assembly of MgADP−fluoroaluminate complexes in two catalytic sites of F_1-ATPases compared to assembly of a fluoroaluminate complex in a single catalytic site. Consider that after a single catalytic site of a nucleotide depleted F_1-ATPase had been loaded with MgADP, the $\alpha_{TP}-\beta_{TP}$ catalytic site contains MgADP with the guanidinium of αR^{373} hydrogen bonded to the 2′-hydroxyl of the ribose moiety. Then, following binding of the AlF_4^- complex to the singly loaded catalytic site, the observed slow formation of the MgADP−fluoroaluminate complex would reflect slow rearrangement of the guanidinium of αR^{373} from the ribose moiety of bound ADP to a position near the β-phosphate where it then hydrogen bonds to the bound AlF_4^- complex. In contrast, the guanidinium of αR^{373} in the $\alpha_{DP}-\beta_{DP}$ catalytic site in the $(ADP)_2$−MF_1 crystal structure is already near the β-phosphate of bound ADP. It follows that simultaneous binding of the AlF_4^- complex to the $\alpha_{TP}-\beta_{TP}$ and $\alpha_{DP}-\beta_{DP}$ catalytic sites containing MgADP would promote more rapid assembly of the MgADP−fluoroaluminate complex in the $\alpha_{DP}-\beta_{DP}$ catalytic site coupled to rotation of the γ subunit. Rotation of the γ subunit would then promote rearrangement of the guanidinium of αR^{373} from the ribose of bound ADP in the $\alpha_{TP}-\beta_{TP}$ catalytic site to a position near the β-phosphate of bound ADP more rapidly than observed when only the $\alpha_{TP}-\beta_{TP}$ catalytic site contains MgADP.

On the basis of the behavior of the $\alpha A^{396}C/\gamma A^{22}C$ and $\beta D^{390}C/\gamma S^{90}C$ double mutant subcomplexes of TF_1 described above, it was surprising that after the cross-linked form of the $\alpha V^{371}/\beta R^{337}C$ double mutant had been incubated with 200 μM MgADP followed by addition of $AlCl_3$ and NaF, irreversible inactivation was ∼100-fold slower than that observed with the reduced double mutant. Under these conditions, at least the $\alpha_{TP}-\beta_{TP}$ catalytic site would contain bound MgADP, presumably with the guanidinium of αR^{373} hydrogen bonded to the 2′-hydroxyl of the ribose moiety. To explain the slow observed rate, cross-linking the $\alpha-\beta$ interfaces near the $\alpha_E-\beta_E$ and $\alpha_{DP}-\beta_{DP}$ catalytic sites might freeze the quaternary structure of the enzyme in a manner that severely attenuates rearrangement of the guanidinium of αR^{373} from the ribose to the β-phosphate of bound ADP where it can form hydrogen bonds with the AlF_4^- complex.

Slow rearrangement of the side chain of αR^{373} at the $\alpha_{TP}-\beta_{TP}$ catalytic site may also be responsible for the observation that the cross-linked form of the $\alpha V^{371}C/\beta R^{337}C$ double mutant hydrolyzes substoichiometric ATP with a k_{cat} of 4.5×10^{-2} s^{-1}. This is ∼100-fold slower than the rate of hydrolysis of substoichimetric ATP by the $\alpha_3(\beta R^{337}W)_3\gamma$ subcomplex of TF_1 reported by Masaike et al. (*22*). Although a high-resolution crystal structure of an active F_1-ATPase with empty catalytic sites is not available, the catalytic characteristics of wild-type and mutant $\alpha_3\beta_3\gamma$ subcomplexes of TF_1 indicate that the asymmetric coiled coil of the γ subunit within the central cavity of the $(\alpha\beta)_3$ hexamer of the subcomplexes generates asymmetry of empty catalytic sites (*10*, *24*, *25*). Following binding of MgATP to the empty $\alpha_{TP}-\beta_{TP}$ catalytic site, the rate-limiting step for hydrolysis might be the rate of rearrangement of the side chain of αR^{373} and side chains in the β subunit that include those of βK^{162}, βE^{188}, and βR^{189} from their positions in the empty catalytic site to their functional positions in the transition state. Since αS^{370} and αV^{371} are connected to αR^{373} by an unstructured strand in crystal structures of MF_1, after two $\alpha-\beta$ pairs in the $\alpha V^{371}C/\beta R^{337}C$ double mutant had been cross-linked, the guanidinium of αArg^{373} might rearrange slowly from its position in the empty catalytic site to its functional position in the transition state when MgATP binds to the catalytic site at the $\alpha_{TP}-\beta_{TP}$ interface.

REFERENCES

1. Yoshida, M., Muneyuki, E., and Hisabori, T. (2001) ATP synthase: A marvelous rotary engine of the cell, *Nat. Rev. 2*, 669−677.
2. Abrahams, J. P., Leslie, A. G. W., Lutter, R., and Walker, J. E. (1994) Structure at 2.8 Å resolution of F_1-ATPase from bovine heart mitochondria, *Nature 370*, 621−628.
3. Gibbons, C., Montgomery, M. G., Leslie, A. G. W., and Walker, J. E. (2000) The structure of the central stalk in bovine F_1-ATPase at 2.4 Å resolution, *Nat. Struct. Biol. 7*, 1055−1061.
4. Menz, R. I., Walker, J. E., and Leslie, A. G. W. (2001) Structure of bovine mitochondrial F_1-ATPase with nucleotide bound to all three catalytic sites: Implications for mechanism of rotary catalysis, *Cell 106*, 331−341.
5. Noumi, T., Futai, M., and Kanazawa, H. (1984) Replacement of serine 373 by phenylalanine in the α subunit of *Escherichia coli* F_1-ATPase results in loss of steady-state catalysis by the enzyme, *J. Biol. Chem. 259*, 10076−10079.

6. Noumi, T., Tanniai, M., Kanazawa, H., and Futai, M. (1986) Replacement of arginine 246 by histidine in the β subunit of *Escherichia coli* F_1-ATPase resulted in loss of multi-site ATPase activity, *J. Biol. Chem. 261*, 9196−9201.
7. Parsonage, D., Duncan, T. M., Wilke-Mounts, S., Kironde, F. A. S., Hatch, L., and Senior, A. E. (1987) The defective proton-ATPase of uncD mutants of *Escherichia coli*, *J. Biol. Chem. 262*, 6301−6307.
8. Lee, S.-F., Wilke-Mounts, S., and Senior, A. E. (1992) F_1-ATPase with cysteine instead of serine at residue 373 of the α subunit, *Arch. Biochem. Biophys. 297*, 334−339.
9. Matsui, T., and Yoshida, M. (1995) Expression of wild-type and the Cys-/Trp-less $\alpha_3\beta_3\gamma$ complex of thermophilic F_1-ATPase in *Escherichia coli*, *Biochim. Biophys. Acta 1231*, 139−146.
10. Ren, H., Dou, C., Stelzer, M. S., and Allison, W. S. (1999) Oxidation of the $\alpha_3(\beta D^{311}C/R^{333}C)_3\gamma$ subcomplex of the thermophilic *Bacillus* PS3 F_1-ATPase indicates that only two β subunits can exist in the closed conformation simultaneously, *J. Biol. Chem. 274*, 31366−31372.
11. Penefsky, H. S. (1977) Reversible binding of P_i by beef heart mitochondrial adenosine triphosphatase, *J. Biol. Chem. 252*, 2891−2899.
12. Bandyopadhyay, S., Valder, C. R., Huynh, H. G., Ren, H., and Allison, W. S. (2002) The $\beta G^{156}C$ substitution in the F_1-ATPase from the thermophilic *Bacillus* PS3 affects catalytic cooperativity by destabilizing the closed conformation of the catalytic site, *Biochemistry 41*, 14421−14429.
13. Bandyopadhyay, S., and Allison, W. S. (2004) The Ionic Track in the F_1-ATPase from the Thermophilic *Bacillus* PS3, *Biochemistry 43*, 2533−2540.
14. Bradford, M. M. (1976) A rapid and sensitive method for the quantitation of microgram quantities of protein utilizing the principle of protein-dye binding, *Anal. Biochem. 72*, 248−254.
15. Jault, J.-M., Matsui, T., Jault, F. M., Kaibara, C., Muneyuki, E., Yoshida, M., Kagawa, Y., and Allison, W. S. (1995) The $\alpha_3\beta_3\gamma$ complex of the F_1-ATPase from Thermophilic *Bacillus* PS3 containing the $\alpha D^{261}N$ substitution fails to dissociate inhibitory MgADP from a catalytic site when ATP binds to noncatalytic sites, *Biochemistry 34*, 16412−16418.
16. Lutter, R., Abrahams, J. P., van Raaij, M. J., Todd, R. J., Lundvist, T., Buchanan, S. K., Leslie, A. G. W., and Walker, J. E. (1993) Crystallization of F_1-ATPase from bovine heart mitochondria, *J. Mol. Biol. 229*, 787−790.
17. Kagawa, R., Montgomery, M. G., Braig, K., Leslie, A. G. W., and Walker, J. E. (2004) The structure of bovine F_1-ATPase inhibited by ADP and beryllium fluoride, *EMBO J. 23*, 2734−2744.
18. Drobinskaya, I. Y., Kozlov, I. A., Murataliev, M. B., and Vulfson, E. N. (1985) Tightly bound adenosine diphosphate, which inhibits the activity of mitochondrial F_1-ATPase, is located at the catalytic site of the enzyme, *FEBS Lett. 182*, 419−424.
19. Yoshida, Y., and Allison, W. S. (1986) Characterization of the catalytic and noncatalytic ADP binding sites in the F_1-ATPase from the thermophilic bacterium, PS3, *J. Biol. Chem. 261*, 5714−5721.
20. Matsui, T., Muneyuki, E., Honda, M., Allison, W. S., Dou, C., and Yoshida, M. (1997) Catalytic activity of the $\alpha_3\beta_3\gamma$ complex of F_1-ATPase without noncatalytic nucleotide binding site, *J. Biol. Chem. 272*, 8215−8221.
21. Ren, H., and Allison, W. S. (2000) On what makes γ spin during ATP hydrolysis by F_1, *Biochim. Biophys. Acta 1458*, 221−233.
22. Masaike, T., Muneyuki, E., Noji, H., Kinosita, K., Jr., and Yoshida, M. (2002) F_1-ATPase changes its conformation upon phosphate release, *J. Biol. Chem. 277*, 21643−21649.
23. Dou, C., Grodsky, N. B., Matsui, T., Yoshida, M., and Allison, W. S. (1997) ADP-fluoroaluminate Complexes are formed cooperatively at two catalytic sites of the wild-type and mutant $\alpha_3\beta_3\gamma$ subcomplexes of the F_1-ATPase from the thermophilic *Bacillus* PS3, *Biochemistry 36*, 3719−3727.
24. Kaibara, C., Marsui, T., Hisabori, T., and Yoshida, M. (1996) Structural asymmetry of F_1-ATPase caused by the γ subunit generates a high affinity nucleotide binding site, *J. Biol. Chem. 271*, 2433−2438.
25. Dou, C., Fortes, P. A. G., and Allison, W. S. (1998) The $\alpha_3(\beta Y_{341}W)_3\gamma$ subcomplex of the F_1-ATPase from the thermophilic *Bacillus* PS3 fails to dissociate ADP when MgATP is hydrolyzed at a single catalytic site and attains maximal velocity when three catalytic sites are saturated with MgATP, *Biochemistry 37*, 16757−16764.

BI047694Z